Submitted to J. Phys. Chem. C, 7/31/2022

Short and Long-Time Dynamics of Hydrogen Spillover from a Single Atom Platinum Active Site to the Cu(111) Host Surface

Kaixuan Gu,[1,2] Chen Li,[3] Bin Jiang,[3,] Sen Lin,[2,*] and Hua Guo[1,*]*

[1]*Department of Chemistry and Chemical Biology, University of New Mexico, Albuquerque, NM 87131, USA*

[2]*State Key Laboratory of Photocatalysis on Energy and Environment, College of Chemistry, Fuzhou University, Fuzhou 350002, China*

[3]*Department of Chemical Physics, School of Chemistry and Materials Science, University of Science and Technology of China, Hefei, Anhui 230026, China*

*: corresponding authors: bjiangch@ustc.edu.cn, slin@fzu.edu.cn, hguo@unm.edu

Abstract

Dynamics of the dissociative chemisorption of H_2 (D_2) and the subsequent H* (D*) diffusion on the Pt dopped Cu(111) surface are investigated using both quasi-classical trajectory (QCT) and ring polymer molecular dynamics (RPMD) approaches. The classical dynamics is also studied with electronic friction to simulate the nonadiabatic interaction with surface electron-hole pairs. These dynamics calculations were made possible by a high-dimensional potential energy surface, machine learned from density functional theory data. It is shown that the diffusion of adsorbed H* at moderate temperatures can be largely characterized by classical mechanics, as evidenced by roughly the same diffusion coefficients obtained from QCT and RPMD calculations. In the long-time limit, the diffusion coefficient computed by averaging classical trajectories with electronic friction is in reasonably good agreement with the latest experimental data, underscoring the importance of the nonadiabatic interaction for H* diffusion on metal surfaces.

I. Introduction

Migration of adsorbed species on catalyst surfaces is a pervasive phenomenon in many heterogeneous catalytic processes. An adsorbed species generated on one surface site can migrate to another site to enable the generation of desired products under more favorable conditions. Hydrogen spillover, where the mobile species is adsorbed atomic hydrogen (H*), has been known for a long time[1] and is continue to receive much attention.[2-4] Hydrogenation catalysts can be designed with one component that is conducive to H* production via for example H_2 dissociation and another component for the subsequent hydrogenation step. Such multi-component catalysts have been pioneered by Sykes and coworkers using single-atom alloys (SAAs), in which the former (platinum group metals, PGMs, such as Pt) is atomically dispersed in the latter (e.g., Cu).[5-12] For example, Lucci et al.[13] designed γ-Al_2O_3-supported Pt/Cu(111) SAA nanoparticle (NP) catalysts, which exhibit high activity and selectivity for butadiene hydrogenation to butene at the temperatures from 30 to 160 ^oC. The catalysis is attributed to the facile dissociation of H_2 at the single atom Pt sites, followed by H spillover to Cu sites where hydrogenation takes place. It is well established that Pt catalyzes H_2 dissociation much more effectively than Cu,[14-15] but the latter is known to effectively catalyze hydrogenation.[16-17] The SAA design has thus the best of both worlds.

For these systems, the transfer of H species from one component to another becomes a key issue. Sykes and co-workers have conducted extensive studies to gain a

better understanding of the H spillover on SAA surfaces.[6-12] By using scanning tunneling microscopy (STM), they reported the appearance of H* atoms on Cu sites after dosing a Pd/Cu(111) SAA surface with H_2 at various temperatures.[18] Diffusion up to ~10^2 nm has been seen even at low temperatures.[8] Similar effects were found for atomically dispersed Pt on Cu surfaces.[11-12] However, very little is known about the dynamics of spillover following the initial H_2 dissociation. In general, one can envision initial rapid hopping of hot H* atoms immediately after dissociation, accompanied by energy dissipation. After reaching thermal equilibrium with the surface, the adsorbed H* undergoes thermal diffusion.

Theoretically, the lowering of the H_2 dissociation barrier on Cu surfaces by PGM dopants have been confirmed by DFT calculations.[19-23] In a recent publication, we discussed the initial H_2 dissociation and subsequent spillover dynamics of H* on a Pt/Cu(111) SAA surface, using ab initio molecular dynamics (AIMD).[24] Following the dissociation at the Pt site, we observed that one hydrogen typically undergoes facile hopping from the Pt site to Cu sites with increasing distances, similar to the behavior observed in the earlier theoretical work on Pd/Cu(111) by Busnengo and coworkers.[19] However, our study suggested that the characteristic diffusion time and length of the adsorbed H* atom are strongly influenced by the interaction with the surface electron-hole pairs (EHPs).[24] The resulting electronic friction (EF) slows the spillover significantly, underscoring the importance of nonadiabatic effects.[25-28] Indeed, the importance of electronically nonadiabatic dissipation in H* diffusion in metals has been noticed before using model potentials.[29-30] More recently, nonadiabatic energy

dissipation of H atoms in scattering from metal surfaces was observed experimentally and characterized theoretically.[31-32] Theoretical predictions of nonadiabatic energy dissipation for hot H* atoms on various metal surfaces have also been made by several groups.[33-35]

Unfortunately, only a few AIMD and AIMD-EF trajectories were calculated in our earlier work[24] and the length of propagation was limited by high computational costs. In addition, nuclear quantum effects such as tunneling are not included in the classical dynamics. This is an important issue that has attracted much recent attention.[10, 36-37] A more in-depth understanding of H spillover on SAA catalyst surfaces requires a better understanding of the impact of nuclear quantum effects and nonadiabatic EHPs. In this work, we extend our previous AIMD work by constructing a high-dimensional potential energy surface (PES) for this system, followed by the modeling of the initial dissociation and subsequent diffusion dynamics using both classical and approximate quantum methods. This PES is based on a periodic model that contains not only the hydrogen coordinates, but also coordinates of surface Pt and Cu atoms, hence capable of handling adiabatic dissipation to the surface phonons and temperature effects. It takes the embedded atom neural network (EANN)[38] form and was trained with the previous AIMD results, augmented by additional calculations reported in this work. By avoiding the expensive DFT calculations in AIMD, the machine learned PES permits efficient calculations of many more quasi-classical trajectories (QCT) for much longer times.[39-40] We address two questions in the current work. First, is there strong nuclear quantum effects in the H spillover at moderate temperatures? To this end, we take advantage of

the ring-polymer molecular dynamics (RPMD) method to describe the dynamics. The RPMD is a path-integral formulation,[41] which can approximately treat nuclear quantum effects in dynamic events, such as hydrogen diffusion.[36-37] However, it is based on classical trajectories of the ring-polymer, thus numerically efficient. The second question is how the nonadiabatic effects via the surface EHPs affect the spillover in both the short- and long-time limits. This question is addressed by comparing QCT results with and without EF on the analytic PES.

II. Methods

IIA. PES

The H_2 + Pt/Cu(111) PES was constructed by the embedded atom neural network (EANN) approach.[38] The training data were obtained from our earlier AIMD calculations,[24] in which the SAA surface was modeled as periodic slabs separated by a vacuum space of 16 Å. Each slab consisted of four atomic layers of Cu(111) with the bottom two layers fixed. The 5 × 5 unit cell had one surface Cu substituted by Pt. The plane wave basis for the valence electrons had a cutoff energy of 400 eV, while the electron-core interaction was approximated with the projector augmented wave scheme.[42] The electron exchange-correlation was described by the optPBE-vdW functional including dispersion effects.[43] Additional DFT calculations were carried out with the same protocol in the current study to supplement the earlier study. All spin-polarized DFT calculations were performed using the Vienna Ab initio Simulation Package (VASP).[44-45]

EANN is an atomistic neural network method for constructing high-dimensional PESs.[38] Specifically, the total energy of the system is expressed as the sum of atomic energies, each of which is an output of an atomic neural network whose input vector is the embedded electron density at this atomic position, namely,

$$E = \sum_{i=1}^{N} E_i = \sum_{i=1}^{N} NN_i(\boldsymbol{\rho}^i) . \quad (1)$$

Here, $\boldsymbol{\rho}^i$ is the density-like feature vector of the central atom i and its component is evaluated by the square of a linear combination of Gaussian-type atomic orbitals (GTOs) located at neighbor atoms,

$$\rho^i = \sum_{l_x,l_y,l_z}^{l_x+l_y+l_z=L} \frac{L!}{l_x!l_y!l_z!} \left(\sum_{j\neq i}^{N_c} c_j \varphi_{l_x l_y l_z}^{\alpha,r_s}(\mathbf{r}_{ij}) f_c(\mathbf{r}_{ij})\right)^2 . \quad (2)$$

Here, N_c is the number of atoms within a cutoff radius (r_c) to the central atom, $f_c(\mathbf{r}_{ij})$ is a cutoff function to ensure that the contribution of each neighbor atom decays smoothly to zero at r_c, c_j serves like an orbital coefficient of atom j that is element-dependent and optimized along with the training process. $\varphi_{l_x l_y l_z}^{\alpha,r_s}(\mathbf{r}_{ij})$ represent GTOs,

$$\varphi_{l_x l_y l_z}^{\alpha,r_s}(\mathbf{r}_{ij}) = x^{l_x} y^{l_y} z^{l_z} exp(-\alpha|r_{ij} - r_s|^2) , \quad (3)$$

where $\mathbf{r}_{ij}$=(x, y, z) is the Cartesian coordinate vector of the neighbor j relative to the embedded atom i with r_{ij} being its norm, α and r_s are parameters that determine radial distribution of the GTO, while $l_x + l_y + l_z = L$ specifies the orbital angular momentum (L) and the angular distribution of the GTO. As can be seen in Eq. (2), an advantage of

the EANN method is that it scales linearly with respect to N_c in the local environment and thus very efficient for including the numerous surface atoms.

15000 points were first generated from the AIMD trajectories to obtain an initial fitting of the PES. QCT calculations were then preformed on the preliminary PES to identify regions in the configuration space where additional points are needed. Additional DFT points, calculated with the same protocol, were then added to the training data. The final PES was constructed by using 18000 points.

IIB. QCT and QCT-EF

The positions and momenta of surface atoms were first sampled from an NVT simulation with an Anderson thermostat.[46] After equilibration of ~3 ps, the simulation at the desired temperature was run for 10 ps, from which surface configurations were saved for the later QCT calculations. The impinging H_2(v=0, j=0) was simulated along the surface normal within a circle centered at the Pt site with a radius of r = 1.4 Å, since the reactivity drops to zero outside the circle due to the high barrier at Cu sites, as discussed in our previous work.[24] The initial position of the impinging H_2 was placed 6.0 Å above the surface with its azimuthal orientation randomly sampled. Several moderate incident energies were adopted in our work, but as shown below, the diffusion of adsorbed H* atoms is not sensitively dependent on the incidence energy, even though the dissociation probability increases with the incidence energy. The initial vibrational and rotational states of the H_2 molecule were sampled from a Boltzmann distribution at several experimental temperatures (200 and 300 K).[11, 13] The time step of 0.10 fs was

used with the velocity Verlet algorithm, which was sufficient to converge the results.

To include the nonadiabatic dissipation due to interactions with surface EPHs, we have also carried out QCT-EF calculations.[26] In such a perturbative EF treatment, the Newton's equation in QCT is replaced by a generalized Langevin equation with an additional friction term, counterbalanced with a fluctuation term.[47] The EF model is based on the independent atom approximation (IAA) version[48] of the local density friction approximation (LDFA).[29, 49] The IAA approximation is appropriate here because the H motion is investigated here. In particular, the interaction with EPHs was approximated by a local density model, in which the friction coefficient of the H* atom is determined by the embedded electron density of the bare surface. The surface electron density was represented in the same EANN method from 800 sampled configurations. The QCT-EF calculations were carried out using the same initial conditions as the QCT calculations.

All QCT and QCT-EF calculations were performed using the VENUS code,[50] which has been heavily modified for surface dynamics.[51] To describe the fates of the impinging H_2, a trajectory was classified as (I) "dissociation", if the H−H distance reached 2.3 Å; or (II) "scattering", if the H_2 is scattered beyond 6.0 Å above the surface with the molecular center velocity pointing away from the surface. An H* atom is classified as (III) "diffusion", if the distance between the H* atom and the Pt site reached beyond 3.2 Å after H_2 dissociation; or (IV) "trapping", if the distance between the H* atom and the Pt site was less than 3.2 Å after H_2 dissociation when the

propagation time of 3 ps was reached. Note that the maximal fraction of diffusion is twice that of the dissociation, because the latter produces two H* adsorbates on the surface. Subsequently, the trajectories were propagated to the final time of 100 ps to extract information about thermal diffusion.

IIC. RPMD

The original RPMD approach was applied to approximate the quantum partition function of a physical system with the ansatz of quantum-classical correspondence,[52] giving rise to an isomorphic ring polymer Hamiltonian. In RPMD, each quantum atom is approximated by a ring polymer consisting of harmonically connected beads. This path integral based method is capable of capturing nuclear quantum effects such as tunneling and zero-point energy,[41] and has been used to investigate H* diffusion on metal surfaces.[36-37]

More recently, Welsch et al. extended the use of RMPD to calculate correlation functions in non-equilibrium (NE) conditions.[53] To that end, an initial momentum impulse ($\Delta\mathbf{p}$) is added to the equilibrated system at the temperature of T, the non-equilibrium ring polymer Hamiltonian becomes,[53]

$$H_n' = \sum_{i=1}^{N}\sum_{j=1}^{n}\left(\frac{\left|\mathbf{p}_{ij}-\Delta\mathbf{p}_i\right|^2}{2m_i'}+\frac{m_i'}{2}\omega_n^2\left|\mathbf{q}_{ij}-\mathbf{q}_{i(j-1)}\right|^2\right)+\frac{1}{n}\sum_{j=1}^{n}V\left(\mathbf{q}_{1j},\cdots,\mathbf{q}_{Nj}\right). \quad (4)$$

where *i* denotes the particles and *j* the beads. The *n* beads have the mass of $m_i' = m_i/n$, and are connected with the harmonic frequency $\omega_n = nk_BT/\hbar$. Marjollet and Welsch have also used the NE-RPMD approach to calculate the reaction cross sections in the

gas phase.[54] In addition, the non-equilibrium ring polymer Hamiltonian has been used to study gas-surface scattering by some of the current authors[55-56] and by Jiang et al.[57-58] In the present case, the momentum $\Delta p_i = m_i' v$ is correlated with the initial translational energy of the impinging H_2 molecule. Following our previous work,[55-56] we sample the Boltzmann distributions of the free H_2 molecule away from the surface by molecular dynamics in contact with a thermostat at the experimental temperatures, with the center of mass translational energy added in the subsequent scattering calculations. The surface configurations are sampled in the same way as done in the QCT calculations. In RPMD calculations, the position of an H atom is approximated by its centroid. The NE-RPMD approach was performed using our in-house code.

III. Results and Discussion

IIIA. Accuracy of PES

In our previous work,[24] on-the-fly AIMD simulations were carried out to explore the impulsive hydrogen diffusion of H* atoms immediately after their initial dissociation at the active Pt site atomically doped on Cu(111). We found that the hot H* atoms diffuse from the initial dissociation site near Pt to nearby Cu surface sites, and the fraction of diffusion and the diffusing length depend on the available energy acquired in the dissociation. Due to the high computational costs of AIMD calculations, the propagation time of dynamics trajectories in our previous work was on the order of a few picoseconds, sufficient to follow the impulsive dynamics of the hot H* atoms immediately after the dissociation, but far shorter than time needed for thermal

diffusion, which can certainly contribute to spillover. The calculated H* diffusion length is only a few Å, which cannot be directly compared with the spillover length of ~10^2 nm reported in experimental studies.[8] To overcome this bottleneck, we developed a globally accurate high-dimensional PES for both the H_2 dissociation and H* diffusion on the Pt/Cu(111) surface, using the EANN method.[38]

The accuracy of the EANN PES of H_2+Pt/Cu(111)-(5×5) has been quantified in several aspects. The root-mean-square error (RMSE) for the training/validation set is 10.8/11.7 meV in energy per cell (including 52 movable atoms) and 18.8/18.9 meV/Å in atomic forces. The energy profile of the H_2 dissociation and H* diffusion on the Pt/Cu(111) surface of our EANN PES is compared with the corresponding DFT results in Figure 1 and the structural parameters of the stationary points along the reaction path are compared in Table 1. The agreement is generally good.

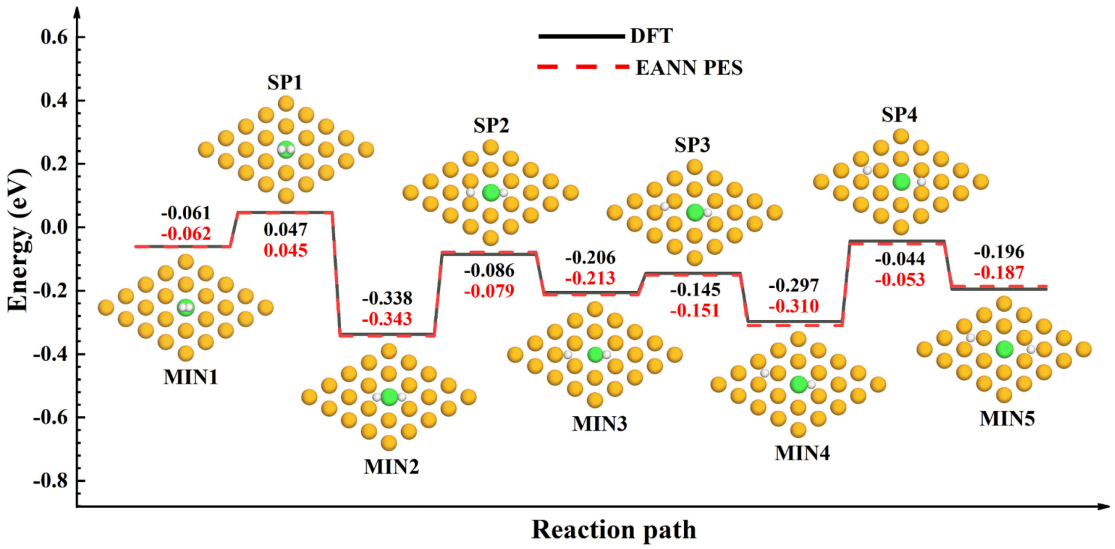

Figure 1. Energy profiles for H_2 dissociation and H* diffusion on the Pt/Cu(111) surface calculated by DFT and EANN PES. Stable adsorption states for the H_2 molecule and H* atoms denoted by potential minima (MIN) and the saddle points (SP) between the minima are presented in the Figure. The energy zero is defined for H_2 far above the surface. White, orange, and green spheres represent H, Cu, and Pt atoms, respectively. For clarity, only the top layer of the Pt/Cu(111) surface is shown.

Table 1. Comparison of the structure parameters of few exemplary potential minima and saddle points obtained from DFT and EANN PES. The H_2 center of mass height Z and internuclear distances between the two hydrogen atoms ($r_{H\text{-}H}$), as well as the in-plane distance between an H* atom and Pt atom ($d_{H\text{-}Pt}$ (Å)), are listed. H_{diff} and H_{trap} represent the diffused H* and trapped H* atoms, respectively.

Configuration	$Site_{Hdiff}$	$Site_{Htrap}$	Z_{Hdiff} (Å)	Z_{Htrap} (Å)	$d_{Hdiff\text{-}Pt}$ (Å)	$d_{Htrap\text{-}Pt}$ (Å)	$r_{H\text{-}H}$ (Å)
MIN1-DFT	Top	Top	3.414	3.414			0.746
MIN1-PES	Top	Top	3.419	3.419			0.745
SP1-DFT	Top	Top	2.132	2.132			0.784
SP1-PES	Top	Top	2.133	2.133			0.786
MIN3-DFT	Hollow	Hollow	1.048	1.272	3.086	1.262	
MIN3-PES	Hollow	Hollow	1.031	1.239	3.090	1.242	
SP3-DFT	Bridge	Hollow	1.172	1.203	3.398	1.293	
SP3-PES	Bridge	Hollow	1.144	1.207	3.400	1.281	
MIN4-DFT	Hollow	Hollow	1.067	1.241	3.985	1.348	
MIN4-PES	Hollow	Hollow	1.018	1.186	3.979	1.349	

The PES in Figure 1 provides an overview of the energy landscape. The dissociation barrier of H_2 at the Pt site (SP1) is 0.108 eV, which is higher than all other saddle points (SP2, SP3, and SP4) and in agreement with previous values (~0.10 eV).[20, 22] The product of the dissociation is a relatively deep minimum with both H* atoms at hollow sites near Pt (MIN2). The PES favors the migration of one H* adsorbate as it hops from one hollow site to another with progressively lower barriers (SP2 and SP3). For the H* diffusion path from MIN3 (hcp site) to MIN4 (fcc site), the barrier is 0.06 eV and the inverse hcp←fcc barrier is 0.15 eV, in agreement with previous calculations using different functionals (~0.14 eV).[37, 59] The migration of the second H* adsorbate

requires a higher barrier (SP4). This potential landscape dictates the dynamics of H spillover discussed below.

IIIB. Dynamics

The availability of an analytical PES allowed us to explore longer time dynamics after the initial dissociation of the impinging H_2 with more trajectories than we did in our previous work. To verify the accuracy of the PES, we have reinvestigated the initial dynamics at the incidence energy of 0.15 eV using the PES and the QCT results are compared with the AIMD result reported in our earlier work.[24] As shown in Table S1 of the Supporting Information (SI), the agreement is satisfactory.

In this work, we performed QCT, QCT-EF, and RPMD calculations on our newly developed EANN PES at the experimental temperatures of 200 and 300 K.[13] The incidence energy of H_2 was chosen to be 0.15 eV along the surface normal. Although several lower energies have been simulated, they do not seem to affect the long-time dynamics, as discussed in Figure S1 of the SI. In the RPMD calculations, 32 and 40 beads were used at 300 and 200 K for all atoms, respectively, and the results are converged with the number of beads, as shown in Figure S2 of the SI. 5000 trajectories were first propagated for QCT, QCT-EF and RPMD. The fractions of the respect channels at the end of the first 3 ps are listed in Table 2.

Table 2. Fractions of H_2 dissociation (f_{diss}), H* trapping (f_{trap}), H* diffusion (f_{diff}) and diffusion length (r) evaluated in the first 3 ps of the QCT, QCT-EF, and RPMD trajectories at 300 and 200 K.

Temperature	Method	f_{diss} (%)	f_{trap} (%)	f_{diff} (%)	r (Å)

300 K	QCT	16.9±0.5	28.2±0.6	5.6±0.3	6.86
	QCT-EF	18.8±0.6	36.6±0.7	0.8±0.1	4.90
	RPMD (32)	28.1±0.6	42.6±0.6	13.7±0.4	6.98
200 K	QCT	15.2±0.5	26.9±0.6	3.4±0.3	6.52
	QCT-EF	18.5±0.6	36.6±0.7	0.3±0.1	4.57
	RPMD (40)	27.6±0.6	52.1±0.7	3.2±0.3	6.17

The initial impact of the impinging H_2 near the Pt dopant could lead to dissociation. Although the lowest dissociation barrier measured from the asymptote is quite small (~0.05 eV), only a fraction of the trajectories results in dissociation, as the barrier increases with the distance from Pt and orientation at impact. The fraction of dissociation is similar for QCT and QCT-EF calculations, indicating that EHPs have only a very limited effect on dissociation. This is consistent with previous studies of the dissociation processes using the LDA model[60-61] or more sophisticated theory.[62-63] It is interesting to note that the dissociation fraction calculated by the RPMD method with 32/40 beads has a significantly larger value. However, this increased dissociation probability should be discounted as the NE-RPMD is known to overestimate the dissociation probability in non-activated dissociative chemisorption processes at low incidence energies.[55] Nonetheless, we expect RPMD to perform well in describing the thermal diffusion process.

For the two H* atoms formed from dissociation, only one typically undergoes diffusion, as observed in earlier simulations.[19, 24] The fraction of diffusion calculated by QCT-EF is much smaller than those obtained using QCT and RPMD, which are proportional to the respective dissociation fractions. The QCT and RPMD diffusion

lengths (r), namely the in-plane distance between the diffusing H* and the initial Pt site, are similar, but significantly larger than the QCT-EF counterpart. These observations indicate that the surface EHPs play a significant role in H* diffusion, due apparently to the rapid energy dissipation of the hot H* atom to the surface. The similarities between the QCT and RPMD diffusion fractions strongly suggest that nuclear quantum effects do not impact the diffusion dynamics in a significant way at these moderate temperatures. These conclusions already reached in our previous study[24] are confirmed with longer time simulations discussed below.

To gain insights into the longer time dynamics, the QCT, QCT-EF and RPMD trajectories at 300 K were propagated further to 100 ps. Since the diffusion fraction for QCT-EF is particularly low, additional 20000 trajectories were added. In Figure 2, the diffusion length (r) is plotted for several exemplary QCT, QCT-EF, and RPMD trajectories. It is shown that the diffusion of the adsorbed H* atom at 300 K is mostly by hopping, evidenced by the sudden change of r followed by a long period of inaction. Such hopping occurs as H* atoms move randomly on the surface, with both increasing and decreasing r. It is not surprising that hopping occurs more frequently immediately after the initial dissociation, due apparently to the high kinetic energy acquired from the dissociation. As the energy of the hot H* atom is gradually dissipated to its surroundings, the frequency of hopping slows down significantly as time progresses. In Figure 3, some exemplary trajectories on the surface plane are shown, which suggest that hopping most occurs between hollow sites on the surface, where the potential minima are located (see Figure 1). Based on the hopping behavior in Figures 2 and 3,

it is clear that the averaged displacement will converge only when many trajectories are averaged. In Table 3, the averaged diffusion length is listed for the three simulation methods and two temperatures.

To characterize the diffusion of adsorbed H* atoms beyond the initial impulsive stage, we compute the diffusion coefficient, which is defined as[64]

$$D = \lim_{\Delta t \to \infty} \frac{<|\Delta r(\Delta t)|^2>}{2d\Delta t} \quad (5)$$

where Δt is the diffusion time, $< |\Delta r(\Delta t)|^2 >$ is the mean square diffusion distance in the time period of Δt, d is the dimension of the system in which diffusion is considered (2 for surface diffusion). An accurate determination of D would require very many trajectories for very long propagation time. In this work, we will limit ourselves to approximate determination of D from a relatively small number (10^3 – 10^4) of trajectories propagated in a relatively short time (10^2 ps). The main aim is not the accurate determination of the diffusion coefficient, but to validate our theoretical models and to gain physical insights into H* diffusion on metal surfaces. In particular, the diffusion coefficients (D) were evaluated based on the assumed linear relationship between the mean square diffusion distance $< |\Delta r(t)|^2 >$ and time. To extract the long-time diffusion coefficient, the time zero is set at 20 ps, to avoid the initial impulsive diffusion, which has a much steeper slope. The time-dependent diffusion coefficients ($D(t)$) are calculated using the data after 40 ps as the validation set according to Einstein's equation $D(t) = \frac{<|\Delta r(t)|^2> - <|\Delta r(t_{20ps})|^2>}{2d(t-t_{20ps})}$. The root mean square error (RMSE) is calculated based on these $D(t)$.

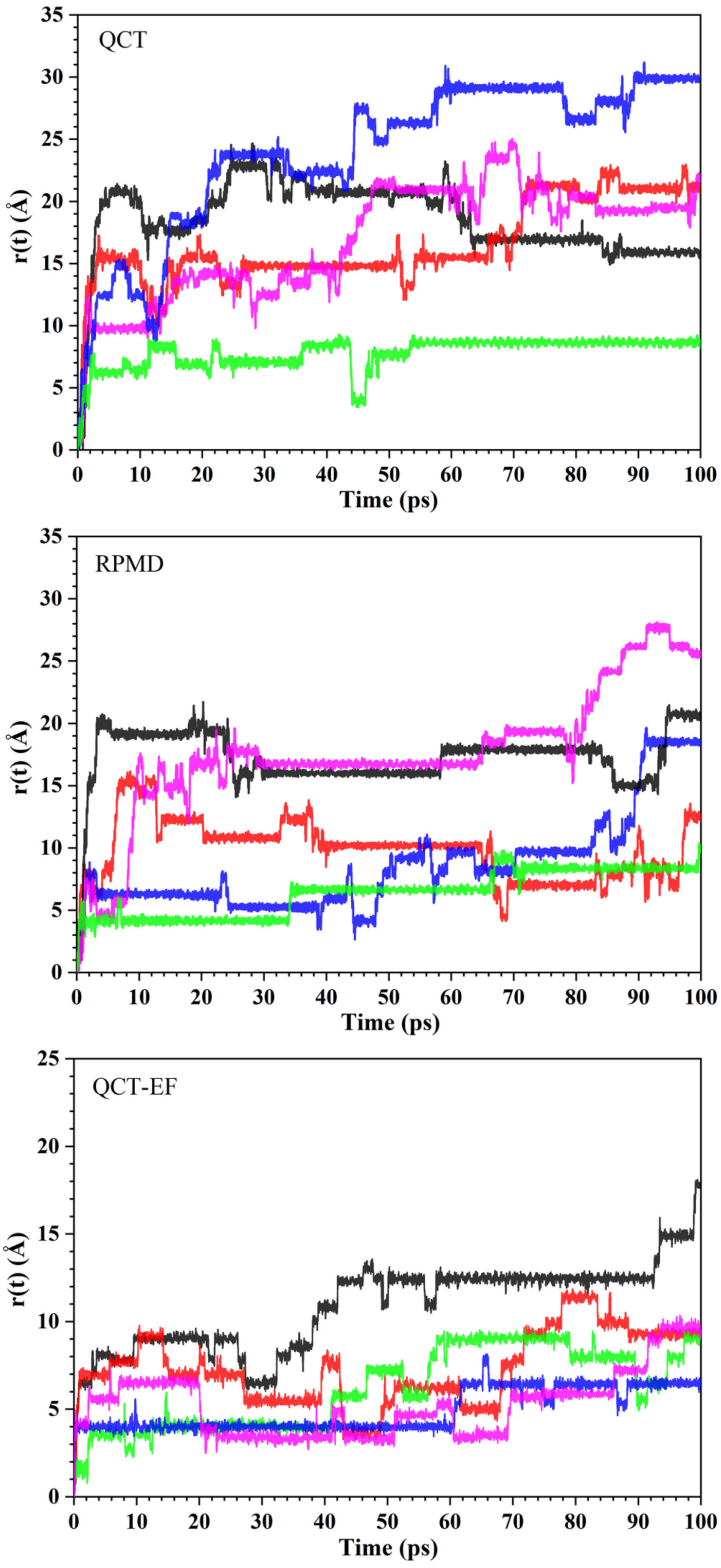

Figure 2. In-plane distances of the diffusing H* from the Pt site (*r*) as a function of

time for several exemplary trajectories calculated using QCT, QCT-EF, and RPMD at 300 K.

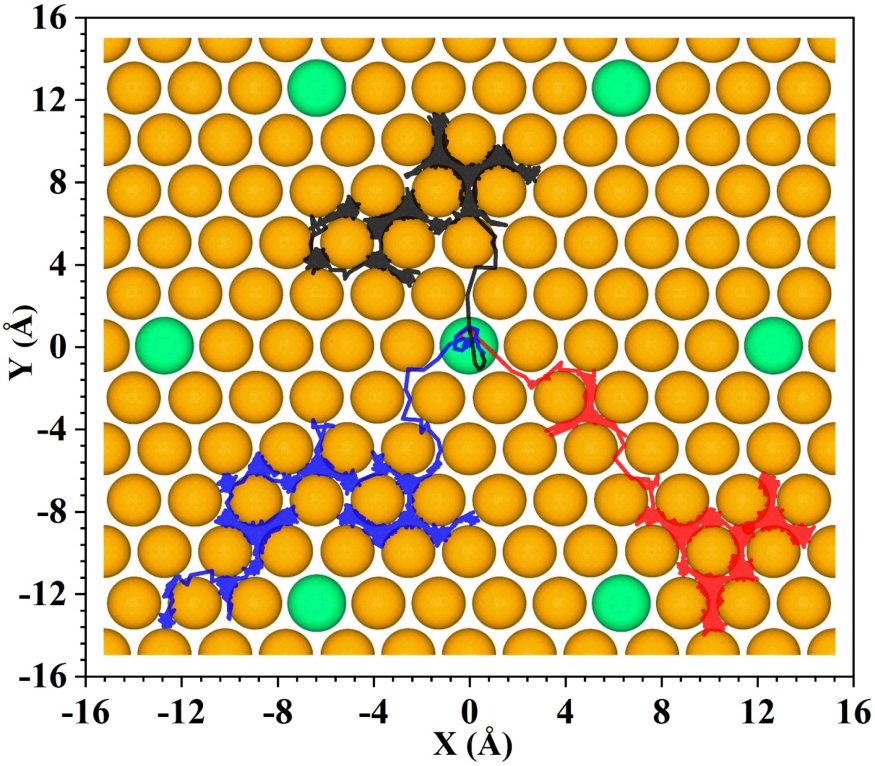

Figure 3. Three exemplary QCT trajectories at 300 K. The H, Cu, and Pt atoms are represented by white, orange, and green spheres, respectively. For clarity, only the top view of the atomic structures is shown.

Table 3. H* diffusion coefficients (D) calculated at the end of the 100 ps simulations using the QCT, QCT-EF, and RPMD methods at 300 and 200 K.

Temperature	Method	D_{theo} (cm^2/s)	D_{expt} (cm^2/s)
300 K	QCT	$(2.9\pm0.2)\times10^{-5}$	
	QCT-EF	$(1.7\pm0.1)\times10^{-5}$	
	RPMD	$(2.6\pm0.2)\times10^{-5}$	
200 K	QCT	$(7.9\pm0.7)\times10^{-6}$	

QCT-EF	$(4.0\pm0.3)\times10^{-6}$	
		$(3.7 \pm 0.3)\times10^{-6}$

In Figure 4, the mean square diffusion distance $< |\Delta r(t)|^2 >$ calculated from the H* diffusion trajectories at 300 K is presented for QCT, QCT-EF, and RPMD as a function of time. These curves in Figure 4 are reasonably smooth after the averaging over the trajectories, due apparently to the finite number of trajectories. As expected, there are clearly two regions: one corresponding to the initial impulsive diffusion of the hot H* atoms (t < 5 ps) and the other is suggestive of conventional diffusion of a thermal H* atom at a longer time scale (t > 20 ps). As expected, the former ballistic diffusion depends sensitively on the initial condition, such as the incidence energy and angle, as shown in our earlier publication.[24] However, the latter self-diffusion has essentially an unchanged diffusion behavior for different initial conditions, also shown in Figure S3 in the SI. The near constant slope in Figure 4 can be used to compute the diffusion coefficient, according to Eq. (5), and the results are listed in Table 3.

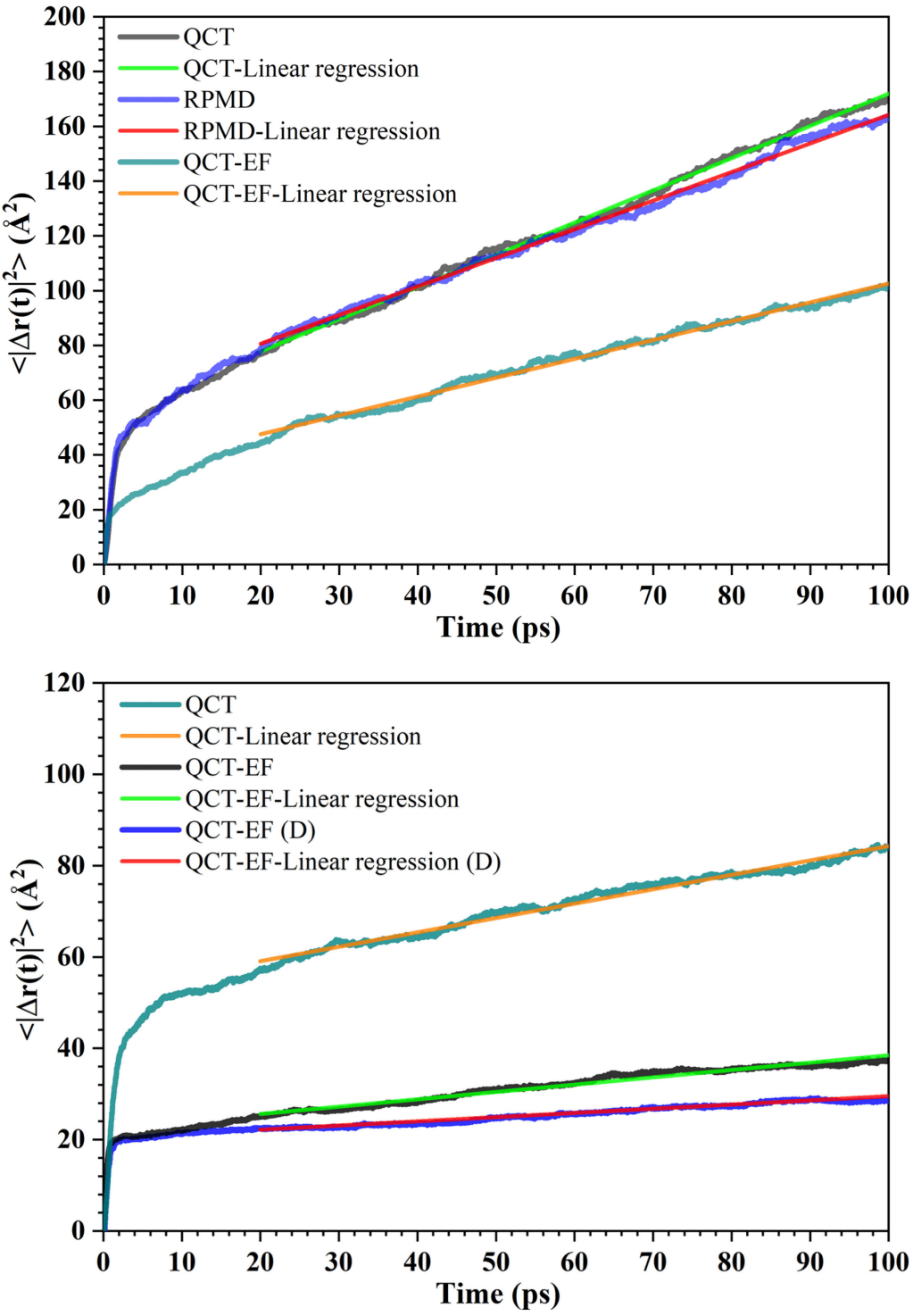

Figure 4. Mean square H* diffusion distances $< |\Delta r(t)|^2 >$ as a function of time calculated by QCT, QCT-EF and RPMD methods at the temperature of 300 (upper panel) and 200 K (lower panel). The fittings are represented by the straight lines. The QCT-EF result for D* diffusion is also included in the lower panel.

From Figure 4, it is easy to see that the $< |\Delta r(t)|^2 >$ curves calculated from QCT and RPMD methods are very similar to each other at 300 K. This is reflected in the diffusion coefficients in Table 3. The roughly the same diffusion behavior within these two models suggest that the H* diffusion at 200-300 K is not significantly influenced by nuclear quantum effects. This is not a surprise as several previous studies have already indicated that nuclear quantum effects only become dominant at much lower temperatures.[37, 65-66] In addition, the calculated diffusion coefficient predicts that it is possible to diffuse 100 nm in about a few microsecond, consistent with the spillover length of ~100 nm reported in recent experimental studies.[8]

Although H spillover is observed in several previous studies on the Pt doped Cu(111) surface, there has been no accurate experimental measurement of the H* diffusion coefficient on this surface. Recently, Townsend et al. reported Helium-3 surface spin echo spectroscopy (HeSE) at the temperature of 200 K,[67] which measured the microscopic hopping rate of H* diffusion on the Cu(111) surface based on a triple jumps model. This allows the deduction of the corresponding diffusion coefficient according to the formula $D = \frac{L^2}{2d} k(T)$,[68] where $k(T)$ is the temperature dependent hopping rate for site-to-site jumps, d is the dimension of the system in which diffusion is considered (d = 2 for surface diffusion), L is distance between hopping adsorption sites. The resulting experimental value of the diffusion coefficient is ~$(3.7 \pm 0.3)\times10^{-6}$ cm^2/s at 200 K, which is included in Table 3. We note that this number is very different from other experimental values,[69-70] which are apparently not accurate as discussed in the work of Townsend.[67]

To assess the accuracy of our calculations, we also performed 100 ps QCT and QCT-EF calculations at 200 K. RPMD trajectories with 40 beads were propagated for 20 ps and the results are very close to that of QCT, as shown in Figure S4 of the SI, so longer RPMD simulations were not carried out as the results are expected to be quite similar to that of QCT, as shown in the 300 K simulations. 5000 trajectories were first propagated for 3 ps in the QCT, RPMD and QCT-EF calculations for a preliminary exploration of H* diffusion behavior and the results are summarized in Table 2. To improve the characterization of H* diffusion, another 3000 and 40000 QCT and QCT-EF trajectories were subsequently added, respectively. These trajectories were propagated to 100 ps to extract the diffusion coefficients, as done for the 300 K simulations.

As shown in Table 3, the QCT result overestimates the measured diffusion coefficient at 200 K by close to 100%, while the QCT-EF value is in reasonable agreement with the experiment. This result suggests that nonadiabatic coupling with the surface EHPs, which slows the H* diffusion, plays an indispensable role. This conclusion should not be a surprise given the recent experimental evidence of nonadiabatic dissipation for H* diffusion through bulk metals.[8, 31] However, this nonadiabatic effect has been ignored in most previous studies of H* diffusion on metal surfaces, which could lead to significant uncertainties in the calculation results.

Finally, we have also performed QCT-EF calculations with 45000 trajectories for D* diffusion at 200 K using the same initial conditions and the results are shown in the

lower panel of Figure 4. The D* diffusion coefficient for extracted from the curve is $(2.3 \pm 0.3)\times10^{-6}$ cm^2/s, which is slightly smaller than that of H*. Currently, there is no reliable experimental data on this property to compare with.

IV. Conclusions

In this work, we have examine the initial dissociation of H_2 (D_2) and subsequent diffusion of H* (D*) atoms on a Pt doped Cu(111) surface, using both classical and approximate quantum methods on a machine learned high-dimensional PES. This PES is not only instrumental in simulation the short and long-time dynamics as reported in this work, it can also be used for investigation of other processes, such as low temperature diffusion coefficients. The dissociation resulted in hot H* atoms which can either be trapped near the Pt site or undergo hopping to nearby Cu sites. Due to rapid energy dissipation to the surface, the H* atoms equilibrate within ~20 ps, and the subsequent dynamics can be described as thermal diffusion. Diffusion coefficients can thus be extracted from the averaged displacement of the H* atoms. Interestingly, the diffusion of H* atom at moderate temperatures (e.g., 300 K) is not significantly affected by nuclear quantum effects. However, the H* diffusion is slowed down by electronic friction due to interaction with surface EHPs, resulting in a better agreement with experiment. Importantly, it is unlikely that this conclusion depends on the functional used in mapping out the PES. Such nonadiabatic interaction is known to slowdown hot H* atoms interacting with metals, but quantum mechanical treatments so far have seldom included such an effect. Our theoretical results presented in this work calls for

more sophisticated theoretical models for characterizing H* diffusion on metal surfaces in the quantum regime, such as in the recent RPMD study with explicit friction tensors.[71] The inclusion of both quantum nuclear effects and electron friction is expected to be necessary for H* diffusion at low temperatures.

Supporting Information: additional results.

Acknowledgements: This work is funded by the National Science Foundation (CHE-1951328 to H. G.). Partial support from National Natural Science Foundation of China (22073089 to B. J. and 21973013 to S.L.), K. C. Wong Education Foundation (GJTD-2020-15 to B.J.), and the National Natural Science Foundation of Fujian Province, China (2020J02025 to S.L.) are also thanked. S.L. also acknowledges the "Chuying Program" for the Top Young Talents of Fujian Province. The calculations were performed at the Center for Advanced Research Computing (CARC) at UNM.

References

1. Khoobiar, S., Particle to Particle Migration of Hydrogen Atoms on Platinum—Alumina Catalysts from Particle to Neighboring Particles. *J. Phys. Chem.* **1964**, *68*, 411-412.
2. Sermon, P. A.; Bond, G. C., Hydrogen Spillover. *Catal. Rev.* **1974**, *8*, 211-239.
3. Prins, R., Hydrogen Spillover. Facts and Fiction. *Chem. Rev.* **2012**, *112*, 2714-2738.
4. Hannagan, R. T.; Giannakakis, G.; Flytzani-Stephanopoulos, M.; Sykes, E. C. H., Single-Atom Alloy Catalysis. *Chem. Rev.* **2020**, *120*, 12044-12088.
5. Tierney, H. L.; Baber, A. E.; Sykes, E. C. H., Atomic-Scale Imaging and Electronic Structure Determination of Catalytic Sites on Pd/Cu near Surface Alloys. *J. Phys. Chem. C* **2009**, *113*, 7246-7250.
6. Tierney, H. L.; Baber, A. E.; Kitchin, J. R.; Sykes, E. C. H., Hydrogen Dissociation and Spillover on Individual Isolated Palladium Atoms. *Phys. Rev. Lett.* **2009**, *103*, 246102.
7. Baber, A. E.; Tierney, H. L.; Lawton, T. J.; Sykes, E. C. H., An Atomic-Scale View of Palladium Alloys and Their Ability to Dissociate Molecular Hydrogen. *ChemCatChem* **2011**, *3*, 607-614.
8. Jewell, A. D.; Peng, G.; Mattera, M. F. G.; Lewis, E. A.; Murphy, C. J.; Kyriakou, G.; Mavrikakis, M.; Sykes, E. C. H., Quantum Tunneling Enabled Self-Assembly of Hydrogen Atoms on Cu(111). *ACS Nano* **2012**, *6*, 10115-10121.
9. Marcinkowski, M. D.; Jewell, A. D.; Stamatakis, M.; Boucher, M. B.; Lewis, E. A.; Murphy, C. J.; Kyriakou, G.; Sykes, E. C. H., Controlling a Spillover Pathway with the Molecular Cork Effect. *Nat. Mat.* **2013**, *12*, 523-528.
10. Kyriakou, G.; Davidson, E. R. M.; Peng, G.; Roling, L. T.; Singh, S.; Boucher, M. B.; Marcinkowski, M. D.; Mavrikakis, M.; Michaelides, A.; Sykes, E. C. H., Significant Quantum Effects in Hydrogen Activation. *ACS Nano* **2014**, *8*, 4827-4835.
11. Lucci, F. R.; Marcinkowski, M. D.; Lawton, T. J.; Sykes, E. C. H., H_2 Activation and Spillover on Catalytically Relevant Pt–Cu Single Atom Alloys. *J. Phys. Chem. C* **2015**, *119*, 24351-24357.
12. Réocreux, R.; Kress, P. L.; Hannagan, R. T.; Çınar, V.; Stamatakis, M.; Sykes, E. C. H., Controlling Hydrocarbon (De)Hydrogenation Pathways with Bifunctional Ptcu Single-Atom Alloys. *J. Phys. Chem. Lett.* **2020**, *11*, 8751-8757.
13. Lucci, F. R.; Liu, J.; Marcinkowski, M. D.; Yang, M.; Allard, L. F.; Flytzani-Stephanopoulos, M.; Sykes, E. C., Selective Hydrogenation of 1,3-Butadiene on Platinum-Copper Alloys at the Single-Atom Limit. *Nat. Commun.* **2015**, *6*, 8550.
14. Luntz, A. C.; Brown, J. K.; Williams, M. D., Molecular Beam Studies of H_2 and D_2 Dissociative Chemisorption on Pt(111). *J. Chem. Phys.* **1990**, *93*, 5240-5246.
15. Kammler, T.; Küppers, J., Interaction of H Atoms with Cu(111) Surfaces: Adsorption, Absorption, and Abstraction. *J. Chem. Phys.* **1999**, *111*, 8115-8123.
16. Zhao, B.; Zhang, R.; Huang, Z.; Wang, B., Effect of the Size of Cu Clusters on Selectivity and Activity of Acetylene Selective Hydrogenation. *Appl. Catal. A* **2017**, *546*, 111-121.
17. Yang, B.; Burch, R.; Hardacre, C.; Hu, P.; Hughes, P., Selective Hydrogenation of

Acetylene over Cu(211), Ag(211) and Au(211): Horiuti–Polanyi Mechanism Vs. Non-Horiuti–Polanyi Mechanism. *Catal. Sci. Tech.* **2017**, *7*, 1508-1514.
18. Kyriakou, G.; Boucher, M. B.; Jewell, A. D.; Lewis, E. A.; Lawton, T. J.; Baber, A. E.; Tierney, H. L.; Flytzani-Stephanopoulos, M.; Sykes, E. C. H., Isolated Metal Atom Geometries as a Strategy for Delective Heterogeneous Hydrogenations. *Science* **2012**, *335*, 1209.
19. Ramos, M.; Martínez, A. E.; Busnengo, H. F., H_2 Dissociation on Individual Pd Atoms Deposited on Cu(111). *Phys. Chem. Chem. Phys.* **2012**, *14*, 303-310.
20. Fu, Q.; Luo, Y., Catalytic Activity of Single Transition-Metal Atom Doped in Cu(111) Surface for Heterogeneous Hydrogenation. *J. Phys. Chem. C* **2013**, *117*, 14618-14624.
21. Fu, Q.; Luo, Y., Active Sites of Pd-Doped Flat and Stepped Cu(111) Surfaces for H_2 Dissociation in Heterogeneous Catalytic Hydrogenation. *ACS Catal.* **2013**, *3*, 1245-1252.
22. Lv, C.-Q.; Liu, J.-H.; Guo, Y.; Wang, G.-C., Selective Hydrogenation of 1,3-Butadiene over Single Pt1/Cu(1 1 1) Model Catalysts: A Dft Study. *Appl. Surf. Sci.* **2019**, *466*, 946-955.
23. Zhao, G.-C.; Qiu, Y.-Q.; Liu, C.-G., A Systematic Theoretical Study of Hydrogen Activation, Spillover and Desorption in Single-Atom Alloys. *Appl. Catal. A* **2021**, *610*, 117948.
24. Gu, K.; Wei, F.; Cai, Y.; Lin, S.; Guo, H., Dynamics of Initial Hydrogen Spillover from a Single Atom Platinum Active Site to the Cu(111) Host Surface: The Impact of Substrate Electron–Hole Pairs. *J. Phys. Chem. Lett.* **2021**, *12*, 8423-8429.
25. Tully, J. C., Perspective: Nonadiabatic Dynamics Theory. *J. Chem. Phys.* **2012**, *137*, 22A301.
26. Alducin, M.; Díez Muiño, R.; Juaristi, J. I., Non-Adiabatic Effects in Elementary Reaction Processes at Metal Surfaces. *Prog. Surf. Sci.* **2017**, *92*, 317-340.
27. Rittmeyer, S. P.; Bukas, V. J.; Reuter, K., Energy Dissipation at Metal Surfaces. *Adv. Phys. X* **2018**, *3*, 1381574.
28. Jiang, B.; Guo, H., Dynamics in Reactions on Metal Surfaces: A Theoretical Perspective. *J. Chem. Phys.* **2019**, *150*, 180901.
29. Li, Y.; Wahnström, G., Nonadiabatic Effects in Hydrogen Diffusion in Metals. *Phys. Rev. Lett.* **1992**, *68*, 3444-3447.
30. Tao, G., Modulating Hydrogen Diffusion on Metal Surfaces by Nonadiabatic Transitions. *AIP Adv.* **2019**, *9*, 065101.
31. Bünermann, O.; Jiang, H.; Dorenkamp, Y.; Kandratsenka, A.; Janke, S. M.; Auerbach, D. J.; Wodtke, A. M., Electron-Hole Pair Excitation Determines the Mechanism of Hydrogen Atom Adsorption. *Science* **2015**, *350*, 1346-1349.
32. Janke, S. M.; Auerbach, D. J.; Wodtke, A. M.; Kandratsenka, A., An Accurate Full-Dimensional Potential Energy Surface for H–Au(111): Importance of Nonadiabatic Electronic Excitation in Energy Transfer and Adsorption. *J. Chem. Phys.* **2015**, *143*, 124708.
33. Galparsoro, O.; Pétuya, R.; Juaristi, J. I.; Crespos, C.; Alducin, M.; Larrégaray, P., Energy Dissipation to Tungsten Surfaces Upon Eley–Rideal Recombination of N_2 and

H_2. *J. Phys. Chem. C* **2015**, *119*, 15434-15442.
34. Galparsoro, O.; Petuya, R.; Busnengo, F.; Juaristi, J. I.; Crespos, C.; Alducin, M.; Larregaray, P., Hydrogen Abstraction from Metal Surfaces: When Electron-Hole Pair Excitations Strongly Affect Hot-Atom Recombination. *Phys. Chem. Chem. Phys.* **2016**, *18*, 31378-31383.
35. Zhou, L.; Jiang, B.; Alducin, M.; Guo, H., Communication: Fingerprints of Reaction Mechanisms in Product Distributions: Eley-Rideal-Type Reactions between D and Cd_3/Cu(111). *J. Chem. Phys.* **2018**, *149*, 031101.
36. Suleimanov, Y. V., Surface Diffusion of Hydrogen on Ni(100) from Ring Polymer Molecular Dynamics. *J. Phys. Chem. C* **2012**, *116*, 11141-11153.
37. Fang, W.; Richardson, J. O.; Chen, J.; Li, X.-Z.; Michaelides, A., Simultaneous Deep Tunneling and Classical Hopping for Hydrogen Diffusion on Metals. *Phys. Rev. Lett.* **2017**, *119*, 126001.
38. Zhang, Y.; Hu, C.; Jiang, B., Embedded Atom Neural Network Potentials: Efficient and Accurate Machine Learning with a Physically Inspired Representation. *J. Phys. Chem. Lett.* **2019**, *10*, 4962-4967.
39. Behler, J., Perspective: Machine Learning Potentials for Atomistic Simulations. *J. Chem. Phys.* **2016**, *145*, 170901.
40. Jiang, B.; Li, J.; Guo, H., High-Fidelity Potential Energy Surfaces for Gas Phase and Gas-Surface Scattering Processes from Machine Learning. *J. Phys. Chem. Lett.* **2020**, *11*, 5120-5131.
41. Habershon, S.; Manolopoulos, D. E.; Markland, T. E.; Miller III, T. F., Ring-Polymer Molecular Dynamics: Quantum Effects in Chemical Dynamics from Classical Trajectories in a Extended Phase Space. *Annu. Rev. Phys. Chem.* **2013**, *64*, 387-413.
42. Blöchl, P. E., Projector Augmented-Wave Method. *Phys. Rev. B* **1994**, *50*, 17953-17979.
43. Klimeš, J.; Bowler, D. R.; Michaelides, A., Van Der Waals Density Functionals Applied to Solids. *Phys. Rev. B* **2011**, *83*, 195131.
44. Kresse, G.; Furthmuller, J., Efficient Iterative Schemes for Ab Initio Total-Energy Calculations Using Plane Wave Basis Set. *Phys. Rev. B* **1996**, *54*, 11169-11186.
45. Kresse, G.; Furthmuller, J., Efficiency of Ab Initio Total Energy Calculations for Metals and Semiconductors Using Plane Wave Basis Set. *Comp. Mater. Sci.* **1996**, *6*, 15-50.
46. Hu, C.; Lin, Q.; Jiang, B.; Guo, H., Influence of Supercell Size on Gas-Surface Scattering: A Case Study of Co Scattering from Au(111). *Chem. Phys.* **2022**, *554*, 111423.
47. Head-Gordon, M.; Tully, J. C., Molecular Dynamics with Electronic Frictions. *J. Chem. Phys.* **1995**, *103*, 10137-10145.
48. Juaristi, J. I.; Alducin, M.; Díez Muiño, R.; Busnengo, H. F.; Salin, A., Role of Electron-Hole Pair Excitations in the Dissociative Adsorption of Diatomic Molecules on Metal Surfaces. *Phys. Rev. Lett.* **2008**, *100*, 116102.
49. Hellsing, B.; Persson, M., Electronic Damping of Atomic and Molecular Vibrations at Metal Surfaces. *Phys. Scr.* **1984**, *29*, 360-371.
50. Hu, X.; Hase, W. L.; Pirraglia, T., Vectorization of the General Monte Carlo

Classical Trajectory Program Venus. *J. Comput. Chem.* **1991**, *12*, 1014-1024
51. Jiang, B.; Guo, H., Dynamics of Water Dissociative Chemisorption on Ni(111): Effects of Impact Sites and Incident Angles. *Phys. Rev. Lett.* **2015**, *114*, 166101.
52. Craig, I. R.; Manolopoulos, D. E., Quantum Statistics and Classical Mechanics: Real Time Correlation Frunction from Ring Polymer Molecular Dynamics. *J. Chem. Phys.* **2004**, *121*, 3368-3373.
53. Welsch, R.; Song, K.; Shi, Q.; Althorpe, S. C.; Miller, T. F., Non-Equilibrium Dynamics from Rpmd and Cmd. *J. Chem. Phys.* **2016**, *145*, 204118.
54. Marjollet, A.; Welsch, R., Nuclear Quantum Effects in State-Selective Scattering from Ring Polymer Molecular Dynamics. *J. Chem. Phys.* **2020**, *152*, 194113.
55. Liu, Q.; Zhang, L.; Li, Y.; Jiang, B., Ring Polymer Molecular Dynamics in Gas–Surface Reactions: Inclusion of Quantum Effects Made Simple. *J. Phys. Chem. Lett.* **2019**, *10*, 7475-7481.
56. Li, C.; Liu, Q.; Zhang, L.; Li, Y.; Jiang, B., Ring Polymer Molecular Dynamics in Gas-Surface Reactions: Tests on Initial Sampling and Potential Energy Landscape. *Mole. Phys.* **2022**, *120*, e1941367.
57. Jiang, H.; Kammler, M.; Ding, F.; Dorenkamp, Y.; Manby, F. R.; Wodtke, A. M.; Miller, T. F.; Kandratsenka, A.; Bünermann, O., Imaging Covalent Bond Formation by H Atom Scattering from Graphene. *Science* **2019**, *364*, 379-382.
58. Jiang, H.; Tao, X.; Kammler, M.; Ding, F.; Wodtke, A. M.; Kandratsenka, A.; Miller, T. F.; Bünermann, O., Small Nuclear Quantum Effects in Scattering of H and D from Graphene. *J. Phys. Chem. Lett.* **2021**, *12*, 1991-1996.
59. Kristinsdóttir, L.; Skúlason, E., A Systematic Dft Study of Hydrogen Diffusion on Transition Metal Surfaces. *Surf. Sci.* **2012**, *606*, 1400-1404.
60. Jiang, B.; Alducin, M.; Guo, H., Electron–Hole Pair Effects in Polyatomic Dissociative Chemisorption: Water on Ni(111). *J. Phys. Chem. Lett.* **2016**, *7*, 327-331.
61. Luo, X.; Jiang, B.; Juaristi, J. I.; Alducin, M.; Guo, H., Electron-Hole Pair Effects in Methane Dissociative Chemisorption on Ni(111). *J. Chem. Phys.* **2016**, *145*, 044704.
62. Maurer, R. J.; Jiang, B.; Guo, H.; Tully, J. C., Mode Specific Electronic Friction in Dissociative Chemisorption on Metal Surfaces: H_2 on Ag(111). *Phys. Rev. Lett.* **2017**, *118*, 256001.
63. Spiering, P.; Meyer, J., Testing Electronic Friction Models: Vibrational De-Excitation in Scattering of H_2 and D_2 from Cu(111). *J. Phys. Chem. Lett.* **2018**, *9*, 1803-1808.
64. Allen, M. P.; Tildesley, D. J., *Computer Simulation of Liquids*; Oxford University: Oxford, 1986.
65. Cao, G. X.; Nabighian, E.; Zhu, X. D., Diffusion of Hydrogen on Ni(111) over a Wide Range of Temperature: Exploring Quantum Diffusion on Metals. *Phys. Rev. Lett.* **1997**, *79*, 3696-3699.
66. Firmino, T.; Marquardt, R.; Gatti, F.; Dong, W., Diffusion Rates for Hydrogen on Pd(111) from Molecular Quantum Dynamics Calculations. *J. Phys. Chem. Lett.* **2014**, *5*, 4270-4274.
67. Townsend, P. S. M. Diffusion of Light Adsorbates on Transition Metal Surfaces. University of Cambridge, 2018.

68. Zambelli, T.; Trost, J.; Wintterlin, J.; Ertl, G., Diffusion and Atomic Hopping of N Atoms on Ru(0001) Studied by Scanning Tunneling Microscopy. *Phys. Rev. Lett.* **1996**, *76*, 795-798.
69. Fei, Y. Y.; Zhu, X. D., Surface Diffusion of Hydrogen Atoms on Cu(111) Studied by Optical Diffraction from Hydrogen Density Patterns Formed on Removable Templates of Xenon Monolayers. *Europhys. Lett.* **2006**, *76*, 877-883.
70. Wang, X.; Fei, Y. Y.; Zhu, X. D., Classical and Quantum Diffusion of Hydrogen Atoms on Cu(111). *Chem. Phys. Lett.* **2009**, *481*, 58-61.
71. Litman, Y.; Pós, E. S.; Box, C. L.; Martinazzo, R.; Maurer, R. J.; Rossi, M., Dissipative Tunneling Rates through the Incorporation of First-Principles Electronic Friction in Instanton Rate Theory. I. Theory. *J. Chem. Phys.* **2022**, *156*, 194106.

TOC graphic